Journal of Ovonic Research Vol. 14, No. 5, September – October 2018, p. 395 - 404

INFLUENCE OF Co DOPING ON STRUCTURAL AND OPTICAL PROPERTIES OF CuO NANOPARTICLES

S. SRIVASTAVA[a,*], A. AGARWAL[b]
[a]*United College of Engineering and Research Allahabad-211010, Allahabad, India*
[b]*Department of Physics, Motilal Nehru National Institute of Technology (MNNIT), Allahabad-211004, Allahabad, India*

Amongst the mono oxides of 3d transition elements series, copper oxide (CuO) is unique as it has a square planar coordination of copper by oxygen in the monoclinic structure. Suitable dopants are often mixed with the CuO matrix, which modify its microstructure resulting in a change in its structural, optical and magnetic properties. The structural and optical properties of CuO nanoparticles synthesized by sol-gel technique have been investigated. The doping concentration affects the luminescence and morphological properties of CuO nanoparticles. For Co doped samples the particle size decreases continuously and monoclinic symmetry of the system gets distorted with increase in dopant concentration. The bandgap undergoes a red shift. The broadening of IR bands increases with increase in dopant concentration.

(Received August 3, 2018; Accepted October 17, 2018)

Keywords: Nanoparticles,FESEM,FTIR, XRD

1. Introduction

Owing to their size linked optical properties and electronic structure, metal oxides, such as SnO_2, ZnO and CuO nanocrystals have evolved much interest in recent years [1-5]. Nanomaterials are characterized by a large amount of surfaces and interfaces. Particle size in the nano range and specific crystal morphologies are likely to improve the performance and allow the fine modification of the properties of these nanomaterials [6]. Among the oxides of transition metals, copper oxide (CuO) or cupric oxide nanoparticles are of special interest from scientific point of view. Copper oxide has shown significance in industrial applications, for gas sensors, magnetic storage medium, solar energy transfer and semiconductors [7]. Cupric oxide (CuO) is a p-type semiconductor with a bandgap of 1.85 eV. Exploration of CuO nanoparticles are few compared to other transition metal oxides like ZnO, SnO_2, TiO_2 and Fe_2O_3 making it an interesting material to study. Altering the characteristics of the material by doping of the semiconductor nanoparticles with metal ions is one of the most significant methods [8]. The influence on physical, chemical, and electronic properties of the semiconductors by engineering of bandgap is possible by making use of the accurate dopants. Upgrading in materials characteristic properties using different dopants have been reported by several authors. The bandgap tapering of SnO_2 nanoparticles doped with Ni was found by Ahmed et al. Das et al. observed the change in emission properties of Mn doped Cu_2O nanoparticles [9]. The methods for the preparation of pure and doped nanocrystalline CuO are sonochemical method, sol–gel technique, room temperature one-step solid state reaction method and electrochemical method. In this chapter, preparation of well dispersed CuO nanoparticles has been given. Here the effect of cobalt (Co) doping on the structural and optical properties of CuO nanoparticles has been discussed. The synthesized CuO nanoparticles were investigated against both, pure and doped forms.

*Corresponding author: sanjaysrivastava@united.ac.in

2. Experimental

2.1 Synthesis

The calculated amount of precursors 50 ml of $CuCl_2.H_2O$ (1.7048 gm) and 50 ml $CoCl_2.6H_2O$ solution (0.5982 gm) of variable concentration (0.5at%, 2at%,5at% and 10at%) were mixed and heated under magnetic stirring for 1 hr. Then 100 ml (2.72 gm) of surfactant sodiumdodecyl sulfate (SDS) was mixed in the above solution with constant stirring. Further 50 ml NaOH (0.8 gm) was mixed in the above solution drop wise. The color of the solution turned blue to black resulting in formation of a suspension. The reaction was continued under stirring and heating for another one hour. Then a wet CuO precipitate was achieved. The wet precipitate was washed thrice with ethanol to remove the impurity ions. After washing the precipitate was dried in oven at 60^0C for 24 hours.

2.2Characterization

The structural and optical properties and photoresponse were investigated using Rigaku X-raydiffractometer with Cu-Kα radiation having wavelength λ = 1.5406Å in the 2θ range from 20^o to 80^o. FESEM and TEM were used to carry out morphological analysis and for particle size measurement. EDAX attached with the FESEM was used for compositional analysis. FTIR spectroscopy measurements were carried out on a Perkin Elmer spectrophotometer using KBr pellets. Optical absorbance spectra were taken using Perkin Elmer UV-Vis spectrophotometer at room temperature. The photoresponse of the nanoparticles was obtained using a photoluminescence spectrometer.

3. Results and discussion

3.1X-ray diffraction

The X-ray diffraction patterns of pure copper oxide and Co doped CuO are shown in Fig.1. The peak positions of all the samples exhibit the monoclinic structure of CuO which was confirmed from the JCPDS card no. 801916. No impurity peak or peaks corresponding to the pure cobalt oxide were observed, indicating that cobalt gets incorporated into the copper oxide lattice showing good purity of the final product and single phase sample formation [10]. It is also observed that with increasing cobalt dopant concentration above 0.5at% i.e. reaching up to 10at%, reflection peaks become stronger and narrower.

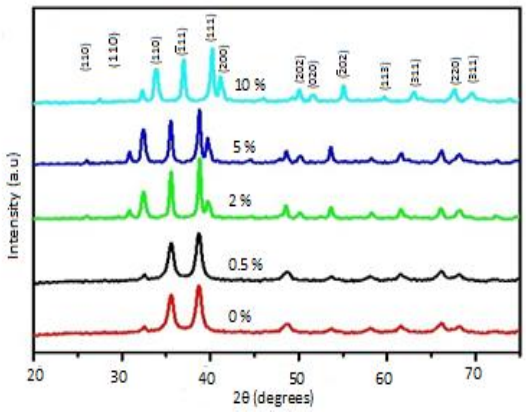

Fig.1. XRD Spectra of pure and Co doped CuO nanoparticles.

Table 1. Variation of crystallite size, lattice parameters and cell volume with dopant concentration.

Dopant Concentration (at%)	Average. Crystallite size (nm)	Lattice parameters			Cell volume ($Å^3$)
		a (Å)	b (Å)	c (Å)	
0	15	4.715	3.428	5.137	81.73
0.5	12	4.713	3.426	5.134	81.68
2	11	4.712	3.426	5.131	81.64
5	10	4.712	3.422	5.128	81.62
10	8	4.702	3.417	5.123	81.28

The crystallite size (D) was calculated using Scherrer formula,

$$D = 0.9\lambda/\beta\cos\theta$$

where λ is the wavelength of X-ray radiation, β is the full width at half maximum (FWHM) of the peaks at the diffracting angle θ. The crystallite size, lattice parameters and cell volume are tabulated in Table1.Lattice parameters shown in the table are very close to the standard lattice parameters reported in JCPDS card no. 801916. It is clear from Table1 that the crystallite size and lattice parameters reduce slightly on increasing dopant concentration, which can be credited to the smaller ionic radii of Co^{2+} (65 pm) ions compared to Cu^{2+} (73 pm) ions [11-12]. It can be seen from XRD spectra that there is no shift in peak positions of Co-doped CuO nanoparticles up to 5at% doping beyond which there is a clear shift in peak positions towards larger angle for 10at% doping indicating no change in the monoclinic symmetry of the system [13-15] with doping up to 5at%. At higher doping concentration (10at %) the shifting indicates a slight distortion in the symmetry of the system due to the creation of defects and vacancies in the system. There is no shift in the peak positions till 5at% and all the diffraction peaks can be assigned to the tetragonalcassiterite CuO phase [16] and preferred orientation (110) that may be followed by (111) plane.

3.2 Scanning electron microscopy and Energy dispersive X-ray spectroscopy

Fig. 2 shows the typical morphology of pure and Co doped CuO nanomaterials. For SEM analysis powder form of the samples were taken. SEM micrographs clearly display the presence of spherical anthology of smaller individual nanoparticles. For CuO sample, the particles are agglomerated to some extent and form lump like structures (Fig. 2 a).The lumping of powders may be due to moisture produced inside the samples [17]. It is seen from the image that lumps have nearly sphere shaped morphology. In the micrographs it is observed that besides spherical morphology, spherical particles transformed into rod shape morphology on the lump of powders when the sample is doped with 2at% of Co (Fig. 2 c). Fine rod shaped morphology is also observed when the doping of Co precursor is increased to 10at% in CuO matrix [18] (Fig. 2 e).

EDAX spectra of pure and Co doped CuO is shown in Fig. 2. It is clear from Fig. 2 (b), (d) & (f) that Co has successfully incorporated in the system [20]. EDAX analysis easily perceives the results revealed from XRD analysis. The ionic radii of Cu^{2+} and Co^{3+} are 0.073 and 0.0685 nm respectively which are within 15% difference and justifies the replacement of Cu ions by Co ions according to Hume-Rothery rule [21-23].

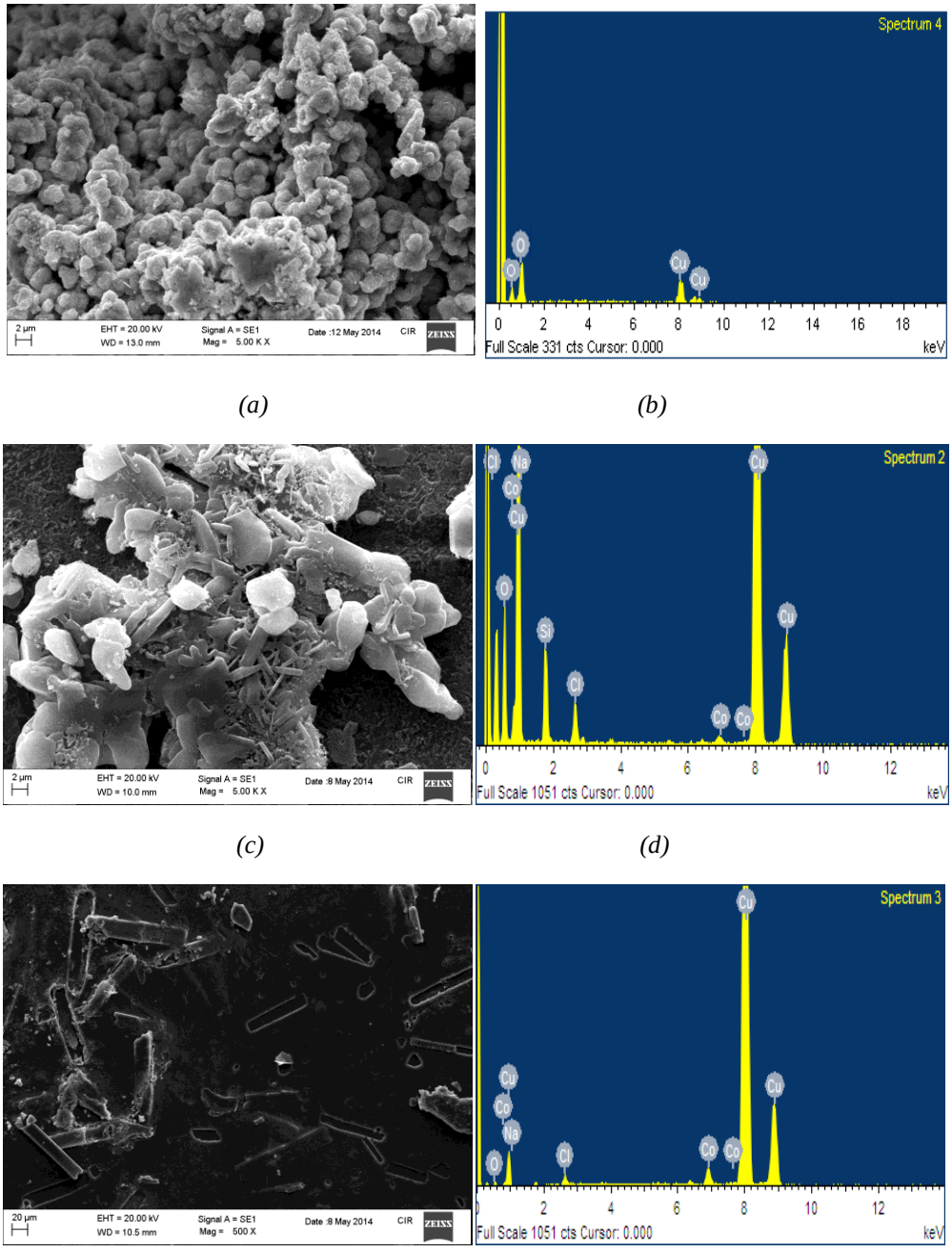

(a) *(b)*

(c) *(d)*

(e) *(f)*

Fig. 2. (a) SEM image of pure CuO(b)EDAX of pure CuO(c) SEM image of 2at% Co doped CuO (d) EDAX 2at% Co doped CuO (e)SEM image of 10at% Co doped CuO(f) EDAX 10at% Co doped CuO.

3.3 Transmission electron microscopy

TEM images are used to study the microstructures of the prepared samples and to measure size of the particles. The particle sizeiation in XRD results were well supported by TEM measurements. TEM micrographs clearly exhibit fine spherical particles for pure CuO nanoparticles and transform into elongated and rod shape structures on increasing Co dopant concentration upto 5at% which is in accordance with the SEM analysis.

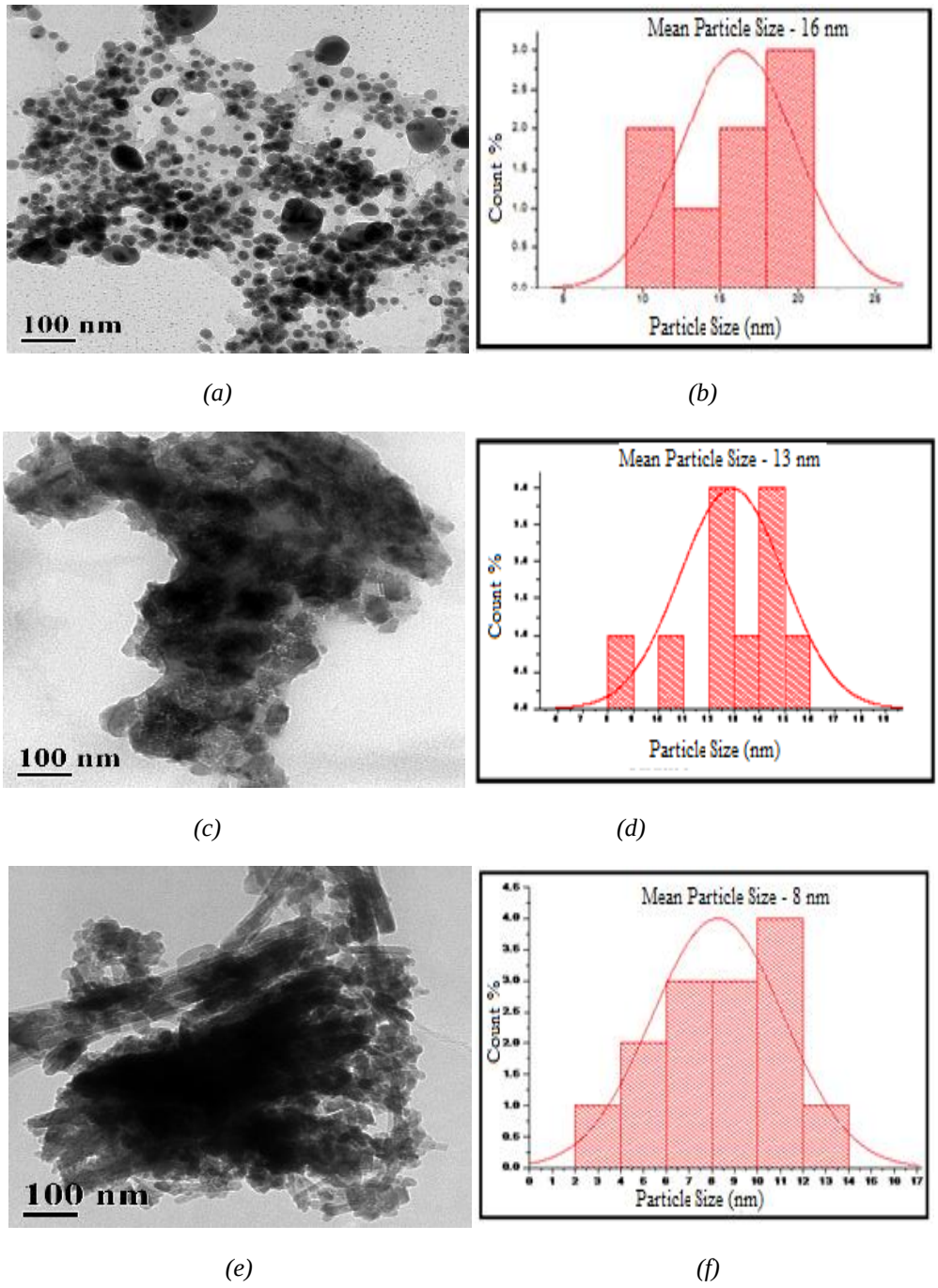

Fig. 3. TEM images of (a) Pure CuO (c) 2at% Co doped CuO (e) 5at% Co doped CuO: Particle size Histogram of (b) Pure CuO (d) 2 at% Co doped CuO (f) 5at% Co doped CuO.

The mean particle size for pure and 2at% Co doped CuO nanoparticles are ~16 nm and ~13 nm which is in well agreement with those of the measurement using XRD pattern. For 5at% Co doping rod-like, wire-like and elongated-shape nanostructures are formed[24].The rod-like nanoparticles of CuO have diameter of the order of 8 nm.The existence of smaller nanoparticles in a verticalgrowth is clearly visible, thus elucidating the fact that the rods themselves may be a result of the accumulation of particles of much smaller dimension [25].

The SAED pattern Fig. 3 (a), (c), (e) features both diffraction spots and a weak ring, indicative of mixed-crystalline structures. SAED pattern for pure sample shows sharp rings with bright spots which indicate good polycrystalline nature of CuO. For doped samples the pattern

exhibits diffused rings with slight sharp boundaries which is indicative of mixed amorphous and polycrystalline nature [26].

3.4 UV-Visible absorption spectroscopy

UV-Visible absorption spectroscopy is one of an important tool to investigate the semiconducting nanoparticles for their optical properties. Absorption spectra of pure and Co doped CuO nanoparticles were taken using Perkin Elmer UV-visible spectrophotometer. The absorption spectra of pure and Co doped CuOnanoparticles are shown in Fig. 4 (a). It exhibits an absorption edge at around 275 nm for all the samples which is smaller than absorbance for bulk CuO which is 310 nm as reported by Zhang et al. This shift towards lower wavelength may be attributed to the quantum confinement effect of nanoparticles. It is interesting to see that the absorption edge is slightly red shifted towards higher wavelength side with increase in doping concentration even the particle size is decreasing with increase in doping concentration, which is in contradiction with the quantum confinement effect.

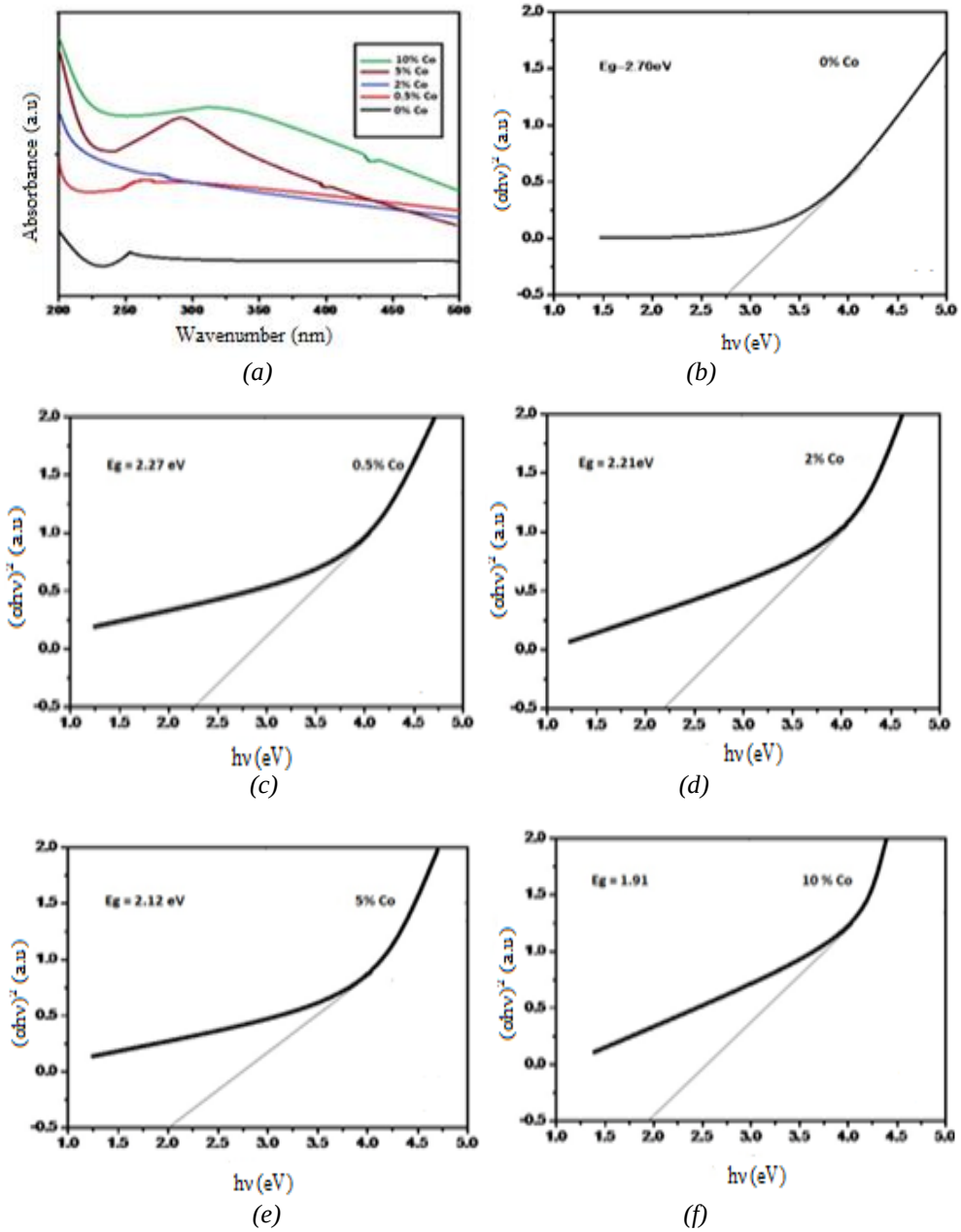

Fig. 4. (a) UV-Visible Absorption Spectra of pure and Co doped CuO (b) Tauc Plot of 0% Co (c) Tauc Plot of 0.5at% Co (d)Tauc Plot of 2at% Co (e) Tauc Plot of 5at% Co (f)Tauc Plot of 10at% Co.

Optical bandgap for all the samples was calculated using well known Tauc relation given by

$$\alpha h\nu = A' h\nu - E_g^n$$

where $\alpha = 2.303A/t$ is called the absorption coefficient A is the absorbance, t is the path length of wave which is equal to the thickness of the cuvette, A′ is the proportionality constant, E_g is the bandgap, hν is the photon energy and n =1/2 and 2 for direct and indirect bandgap semiconductors respectively. It is evident from Tauc plots that bandgap of pure CuO nanoparticles is 2.6 eV which is higher than that of bulk CuO (1.85 eV).It has been observed that the bandgap decreases with Co doping with the decrease in particle size. The red shift in the bandgap can be attributed to the presence of intra gap defects in doped samples [27-28]. This decrease has been attributed to the quantum confinement effect of nanoparticles. Intra gap defects have also been reported to decrease the bandgap of CuO nanoparticles by Rehman et al [29]. Ovchinnikov et al. have discussed the role of electronic defects in CuO. They have observed that the intraband states are developed within the bandgap due to presence of dopants or valence defects (e.g. O vacancies and Cu^{1+} state) in CuO nanoparticles and these are the sources of decrease in the bandgap [30]. Similar decrease in bandgap of Ni doped SnO_2 has also been observed, where bandgap decreases with Ni doping with the reduction in size.

3.5 Fourier transform infrared spectroscopy

Fourier transform infrared (FTIR) spectra were recorded by making use of KBr pellets technique in solid phase in the range of 1000–3500 cm^{-1}. Structural properties of CuO nanoparticles in pure and doped form are shown in Fig.5 using FTIR spectroscopy. All spectra were obtained using powder samples which were dissolved in ethanol to record the spectra in the range of 1000 - 3500 $cm^{-1}$with a resolution of 2 cm^{-1}.

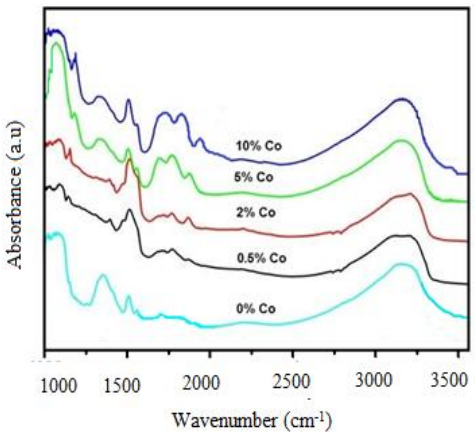

Fig. 5. FTIR spectra of pure and Co doped CuO nanoparticles.

The creation of CuOwurtzite structure is supported through FTIR, in the Co- doped CuO samples [31]. The absorbance spectra shows vibrations in the range 900-1200 cm^{-1}which can be ascribed to the vibrations of Cu-O, confirming the formation of CuO nanoparticles for the undoped CuO as well as the Co-doped CuO samples (Fig. 5). The absorption peaks in the range of 900 - 1200 cm^{-1} could be ascribed to the CuO stretching modes [32]. The observed prominent peaks in the FTIR spectra are, absorption peaks in the range of 1600 - 2100 cm^{-1}correspondto the Cu-OH bending mode and a broad band in the range of 2800 - 3500 cm^{-1} region which is due to overlapping of O-H stretching modes and C-H stretching modes [33], between 2700 and 3000 cm^{-1}.Strong bands for all the samples are observed around this range which can be ascribed to the vibrations of Cu(II)-O bond. The same results have been observed in many semi-conductors,

where local vibrational modes are allocated to the symmetric and antisymmetric C-H broadening modes [34].

It is also observed that broadening of IR bands increases with the increase in doping concentration implying the particle size tend to reduce with doping. H. Zhang et al. have also reported the broadening of IR bands with the decrease in particle size [36]. As the particle size decreases, defects and local lattice distortions appear in the system lowering the crystal symmetry leading to the broadening of FTIR peaks. Similar broadening have also been observed by Fangxin et al. in nanosized ZrO_2 [37].

3.6 Photoluminescencespectroscopy

The room temperature photoluminescence behavior of pure and Co doped CuO nanoparticles was examined using fluorescence spectrophotometer and the results are shown in Fig. 6.Photoluminescence spectra were recorded at an excitation wavelength of 300 nm. A sharp emission band occurred in the UV region at 332 nm, while two emission bands located at 412 nm (visible region) and 440 nm were also investigated. It can be observed thatPL peak positions do not change with Co doping. However, the observed PL signals in the visible region are distinguished with increasing doping concentration. The emission peaks occurred in the visible region can be assigned to the defects and vacancies generated due to either non-stoichiometric or substitution of Co into CuO nanoparticles [37-38]**.** The PL results are also verified with XRD and FTIR analysis as the deviation in XRD peaks of higher concentration of Co doping CuO nanoparticles is responsible for the generation of lattice defects in the system. It is supposed that the emission wavelength of the oxide material depends largely on the particle's shape, size and excitation wavelength [39-40]. The first emission peak at 361 nm can be attributed to the band edge emission. The second weak peak occurred in the visible region can be assigned to the defects and vacancies generated due to non-stoichiometric CuO.

Non stoichiometry is generated in CuO due to the existence of Cu vacancies [41]. The third PL peak occurring at 440 nm was found owing to band impurity transition which results in the recombination of electron bound to donor and free holes. Band impurity transition is also verified from absorbance results where bandgap was found to decrease with doping due to the existence of impurity or defect states within the bandgap. It can be seen from Fig. 6 that there is no change in PL peak positions with doping. However, a slight increase in the intensity of luminescent emission was observed with doping which can be attributed to the defects such as oxygen interstials and Cu vacancies in the doped samples [42].

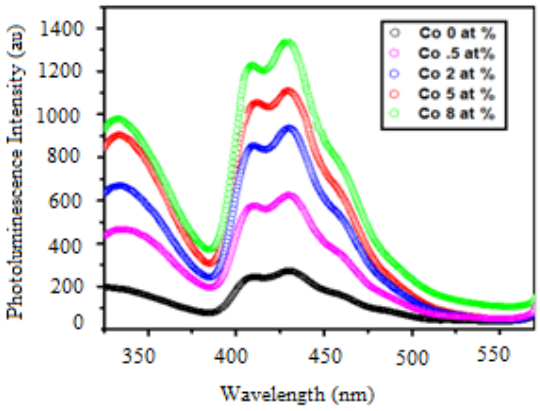

Fig. 6.Photoluminiscence spectra of pure and Co doped CuO nanoparticles.

4. Conclusions

Cobalt-doped CuO nanoparticles were successfully prepared using sol-gel combustion route with Co doping concentration from 0 to 10at%.The XRD patterns confirm the formation of

single phase CuO nanoparticles. The XRD peak relative intensity changes with increasing Co doping concentration with respect to pure CuO nanoparticles. The XRD spectra exhibits that no impurity phase is present in the sample. The decrease in particle size, lattice parameters and cell volume were observed on increasing cobalt concentration. The XRD patterns and SEM micrographs of doping of Co in CuO confirms the development of resultant structure. The EDAX pattern indicates that Co is successfully doped in the CuO nanocrystals. The transmission electron microscope (TEM) measurement presents that the average particle size of Co-doped CuO was found to decrease on increasing the dopant concentration which is in accordance with XRD observations. The bandgap of the doped samples shows a tapering effect as measured from the Tauc relation. The bandgap energy decreases to a large extent from 2.6 eV (pure CuO) to 1.91 eV (10at% Co), due to which there is red shift of wavelength in UV absorption. A broad visible emission peak is observed in PL spectra which may be due to the surface defect levels. The photoluminescent emission intensity slightly increases on increasing the dopant concentration. Thus the current doping method can be regarded as an excellent method to alter the optical properties of CuO nanoparticles and the structural and optical properties of the CuO nanoparticles gets improved due to cobalt doping in CuO.

References

[1]J.G. Hu, T.W. Odom, C.M. Lieber, Acc. Chem. Res. **32**, 435 (1999).
[2]X.F. Duan, Y. Huang, Y. Cui, J.F. Wang, C. M. Lieber, Nature**66**, 409(2001).
[3] M.S. Gudiksen, L.J. Lauhon, J.F. Wang, D.C. Smith, C.M. Lieber,Nature**415**, 617 (2002).
[4] X.F. Duan, Y. Huang, R. Agarwal,C.M. Lieber, Nature **421**, 241 (2003).
[5] P. Yang, C.M. Lieber, Science **273**, 1836(1996).
[6]Neha Topnani, SurendraKushwah,TaimurAthara,International Journal of Green Nanotechnology**1**, 67 (2010).
[7] M. Stefan, S.V. Nistor, D. Ghica, Springer Series in Materials Science **1205**, 44479 (2014).
[8] K. Usharani, A.R. Balu, V.S. Nagarethinam, M. Suganya, Progress in Natural Science: Materials International**10.1016**, 06.003(2015).
[9] A. S. Ahmed, S. M. Muhamed, M.L.Singla, S.Tabassum, A. H.Naqvi, A. Azam, J. Lumin. **131**, 1 (2011).
[10] US. Rai, L. Singh, K. D. Mandal, N. B. Singh,Nanosci. Tehnol. **1**(2), 1 (2014).
[11] J. A. Wasserstein, Soc. Sci. Fenn.**1**(38), 1(1923).
[12] R. D. Shannon, ActaCryst. A**32**, 751(1976).
[13] H. Falcon, A.E. Goeta, G. Punte, R.E. Carbonio, Solid State Chem.**133**, 379 (1997).
[14] V.V. Kharton, A.P. Viskup, E.N. Naumovich, V.N. Tikhonovich, Mater. Res. Bull. **34**, 1311 (1999).
[15] R. Chiba, F. Yoshimura, Y. Sakurai, Solid State Ion.**124**, 281 (1999).
[16] H.Pirmordi,J.Malkootikhah,M App Sc Journal**13**, 1129 (2011).
[17] D.S. Horn, G.L. Messing, Mater. Sci. Eng.**195**, 169 (1995).
[18] Hari Singh Nalwa, Journal of Nanoscience and NanotechnologyISSN: 1533-4880, 1533.
[19] Qing Wan, JiaSun,Huixuan Liu,Semiconducting Oxide Nanowires: Growth, Doping and Device applications, 2011.
[20] W. Smith, J. Hashemi, Foundations of Materials Science and Engineering, 139 (2006).
[21] H. K. D. H. Bhadeshia, Solid Solutions: The Hume-Rothery Rules, Retrieved 2007-11-24.
[22] W. Hume-Rothery, H. M. Powell, Z. Krist.**91**, 23 (1935).
[23] W. Hume-Rothery, Atomic Theory for Students of Metallurgy, The Institute of Metals, London, 1969.
[24] Sarika D. Shinde, G. E. Patil, D. D. Kajale, D. V. Ahire, V. B. Gaikwad, G. H. Jain, Int. Journ.of Sm.Sens. Sys. **5**, 1 (2012).
[25] Y. Zia,De Li, Advance materials research,2004.
[26] Petrova,Urbana, Illinois,P. B. Barna, J. Vac. Sci. Technol. A**21**, 5(2003).

[27] D.I. Son, C.H. You, T.W. Kim, Appl. Surf. Sci. **255**, 8794 (2009).
[28] A.S. Lanje, S.J. Sharma, R.B. Pode, R.S. Ningthoujam, Advances in Applied Science Research**1**, 36 (2010).
[29] S. Rehman, A.Mumtaz, S.K.Hasanain, J. Nanopart. Res.**13**, 2497 (2011).
[30] S.G. Ovchinnikov, B.A. Gizhevskii, Y.P. Sukhorukov, A.E. Ermakov, M.A. Uimin, E.A. Kozlov, Y. Kotov, A.A. V. Bagazeev, Phys Solid State **49**, 1116 (2007).
[31] Najran, ACS Applied Materials & Interfaces, 1346 (2011).
[32] Chowa, O. Lupana, G. Chaia, H. Khallafa, L.K. Onoa, B. Roldan Cuenya, I.M. Tiginyanuf, V. V. Ursakif, V. Sonteac, A. Schultea,Sensors and Actuators, 2012.
[33] Walt Volland Bellevue, Organic Compound Identification Using Infrared Spectroscopy, Washington, 1999.
[34] Tor Karlsen, Leif J. Sæthre, Knut J. Børve, Nora Berrah, Edwin Kukk, John D. Bozek, Thomas X. Carroll,T. Darrah Thomas, J. Phys. Chem. A**105**, 7700 (2001).
[35] Hao Zhang, Yulong Liu, Ke Zhu, Gueigu Siu, YonghongXiong, CaoshuiXiong, HaoZhang et al, J. Phys.: Condens.Matter, 2035 (1999).
[36] A.K.Singh, Umesh T. Nakate, The Scientific World Journal Volume, 2014.
[37] Biswajit Choudhury, MunmunDey, Amarjyoti Choudhury, Choudhury et al., International Nano Letters, 25(2013).
[38] Lianjun Liu, Ying Li, Aerosol and Air Quality Research **14**, 453(2014).
[39] J. Wan, L. Shi, B. Benson, M. J. Bruzek, J. E. Anthony, P. J. Sinko, R. K, H. A. Stone, Langmuir **37**, 13143 (2012)
[40] Neha Singh, Fazila Syed, Fozia Z. Haque,Mat Sc. Res India, 13005 (2012).
[41] Mergoramadhayenty Mukhtar, LusitraMunisa, Rosari Saleh, Materials Sciences and Applications**3**, 543 (2012).
[42] W. J. Liu, X. D. Tang, Z. Tang, W. Bai, N. Y. Tang, Advances in Condensed Matter Physics, 424398 (2013).